Charles University in Prague

Faculty of Mathematics and Physics

BACHELOR THESIS

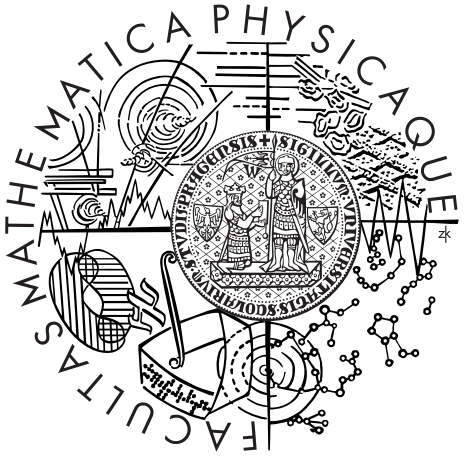

Pavel Malý

Srovnání poruchových a neporuchových přístupů k teorii optické spektroskopie

Institute of physics of Charles University

Supervisor of the bachelor thesis:	RNDr. Tomáš Mančal, Ph.D.
Study programme:	Physics
Specialization:	General physics

Prague 2012

I would like to thank my supervisor Tomáš Mančal for his guidance and also my friends and colleagues for valuable discussions and help with various physical and technical issues.

I declare that I carried out this bachelor thesis independently, and only with the cited sources, literature and other professional sources.

I understand that my work relates to the rights and obligations under the Act No. 121/2000 Coll., the Copyright Act, as amended, in particular the fact that the Charles University in Prague has the right to conclude a license agreement on the use of this work as a school work pursuant to section 60 paragraph 1 of the Copyright Act.

In ..... date ..... signature of the author

Název práce: Porovnání poruchových a neporuchových přístupů k teorii optické spektroskopie

Autor: Pavel Malý

Katedra: Fyzikální ústav Univerzity Karlovy

Vedoucí bakalářské práce: RNDr. Tomáš Mančal, Ph.D., Fyzikální ústav Univerzity Karlovy

Abstrakt: Tato práce je zaměřena na porovnání poruchového a neporuchového výpočtu polarizace třetího řádu ve dvou dimenzionální (2D) optické spektroskopii. Dvouhladinová molekula a vázaný dimer jsou zvoleny jako příklady systémů jejichž 2D spektrum je spočteno s použitím explicitních pohybových rovnic pro redukovanou matici hustoty a integrováním odezvových funkcí. S použitím získaných výsledků jsou tyto dva přístupy porovnány kvalitativně a kvantitativně. Hlavní nalezený rozdíl je přítomnost příspěvků vyšších řádů polarizace v neporuchově vypočteném spektru.

Klíčová slova: Nelineární 2D optická spektroskopie, Poruchový přístup, Neporuchový přístup, Dvouhladinový systém, Dimer

Title: Comparison of perturbative and non-perturbative approaches to optical spectroscopy

Author: Pavel Malý

Department: Institute of physics of the Charles University

Supervisor: RNDr. Tomáš Mančal, Ph.D., Institute of physics of Charles University

Abstract: This thesis focuses on the comparison of perturbative and non-perturbative calculation of the third order polarization in two dimensional (2D) optical spectroscopy. A two-level molecule and a coupled dimer are chosen as simple systems for which the 2D spectrum is calculated using explicit equations of motion for the reduced density matrix and integrating the response functions. The two approaches are compared qualitatively and quantitatively using obtained results. The main difference found is the presence of higher order polarization contributions in non-perturbatively calculated spectrum.

Keywords: Non-linear 2D optical spectroscopy, Perturbative approach, Non-perturbative approach, Two-level system, Dimer

Contents

Introduction

Optical spectroscopy is an excellent tool for revealing the electronic properties of molecular systems. The relatively new type of optical spectroscopy, two-dimensional (2D) non-linear spectroscopy [1, 6], is a cutting-edge technique with high time (down to tens of femtoseconds) and frequency resolution, making it an ideal tool for observing ultrafast processes such as energy transfer or excitonic wavepacket motion [9, 1]. Recently, this method was succesfully applied to various photosynthetic protein complexes such as the Fenna-Matthews-Olson (FMO) antenna complex [3], LH3 antenna complex [18] and other artificial chromophore complexes[12], studying the energy transfer between chromophores. In some cases, a long-lived quantum coherences were found, for FMO even at physiological temperature [15]. Apart from biological systems, 2D spectroscopy can also be used to study materials such as quantum wells [17] or polymers [2]. From appropriately interpreted spectra it is possible to determine resonant transition frequencies, excitonic energy transfer rates, time evolution of coherent superpositions of states and, from the shape of the peaks, the form of the interaction with the molecular environment.

The spectra can be calculated either perturbatively, restricting only to the expected order of perturbation, or non-perturbatively, solving the equations of motion and then extracting the required polarization by so-called phase cycling. The main reason for perturbative approach is its more intuitive nature and easy-to-interpret language of the Feynman diagrams and Liouville space pathways, which correspond to the components of non-linear response functions. However, for more complicated systems the response function formulation becomes more and more complicated as the number of possible Liouville pathways quickly grows beyond feasibility (see for example Figures B.1,B.2). Here, the (numerically) exact solution of equations of motion for the density matrix becomes the choice. The aim of this work is to demonstrate the similarities and differences of these two approaches.

1. Theoretical description

In this chapter, the theoretical and experimental description of non-linear spectroscopy will be outlined [13]. The general equations describing the system of interest in the interaction with external electrical field will be derived and used approximations will be discussed. Briefly, the experimental setup will also be described. The perturbative and non-perturbative approach to the spectrum calculation will be introduced.

1.1 Approach outline

As we are interested in the system dynamics induced by the interaction with an external electric field, we will be working within a semiclassical description, where the molecular system is treated quantum mechanically and the electric field is described on the classical level. The system-field interaction will be treated within the dipole approximation, see Section 1.3. Finally, the reduced description will be used. Typically, we are interested in the spectroscopy of a molecular system S with describable amount of degrees of freedom (DOF) over which we have control. This molecular system is interacting with its environment, which is a large bath B over which we have no control. A molecular system in interaction with its environment is called open quantum system. The Hamiltonian can be then traditionally divided as (the hats for operators will be from now on omitted)

$$H = H_S - \boldsymbol{\mu}\cdot\mathbf{E}(t)+H_{SB} + H_B, \tag{1.1}$$

where H_S is the system Hamiltonian, $\mathbf{E}(t)$ is the electric field, $\boldsymbol{\mu}$ is the dipole moment operator, H_{SB} is the system-bath interaction and H_B is the bath Hamiltonian. To eliminate the unknown dynamics of the bath, we use reduced density matrix (RDM) (W is the ordinary density matrix operator)

$$\rho(t) = Tr_B\{W\}. \tag{1.2}$$

For a simpler description, let us from now on write the scalar product of $\boldsymbol{\mu}$ and $\mathbf{E}(t)$ as its size, $\boldsymbol{\mu}\cdot\mathbf{E}(t) = \mu E(t)$. Here, $\mathbf{E}(t) = \mathbf{e}\cdot E(t)$ and $\mu = \boldsymbol{\mu}\cdot\mathbf{e}$. In dipole approximation, the polarization is the mean value of the dipole operator:

$$P(t) = \langle\mu\rangle = Tr_S\{\mu\rho\}. \tag{1.3}$$

The spectroscopic signal we ultimately want to calculate can be related to the polarization by solving the Maxwell equations. The signal electrical field turns out to be proportional to the polarization:

$$E_S(t) \sim iP(t). \tag{1.4}$$

This means that the desired quantity to compute is the reduced density matrix $\rho(t)$.

Letting the system-bath interaction aside for a moment, from the Schrödinger equation for the system wavefunction we get the so-called Liouville equation for the density matrix

$$\frac{\partial}{\partial t}\rho(t) = -\frac{i}{\hbar}[H_S, \rho(t)] + \frac{i}{\hbar}[\mu, \rho(t)]E(t). \tag{1.5}$$

Or, rewriting within the Liouville space (in which the density matrix lives as a vector) and adding the system-bath interaction [11],

$$\frac{\partial}{\partial t}\rho(t) = -i\mathcal{L}\rho(t) - \mathcal{R}\rho(t) + i\mathcal{V}\rho(t)E(t). \tag{1.6}$$

Here, $\mathcal{R}$ is the relaxation operator (see Section 1.3), $\mathcal{L}$ is the system Liouville operator acting as $\mathcal{L}_S\bullet = \frac{1}{\hbar}[H_S, \bullet]$ and $\mathcal{V}$ is the dipole operator in Liouville space acting in a similar way $\mathcal{V}\bullet = \frac{1}{\hbar}[\mu, \bullet]$.

To see the dynamics of the system-field interaction better, let us include the relaxation operator into the Liouville operator as $\mathcal{L}_0 = \mathcal{L} - i\hbar\mathcal{R}$ and switch to the interaction picture $\rho(t) = \mathcal{U}(t)\rho^I(t)$. Here, $\mathcal{U}(t)$ is a Liouville space propagator $\mathcal{U}(t) = \exp(-i\mathcal{L}_0 t)$. The equation of motion for the density matrix (1.6) now reads

$$\frac{\partial}{\partial t}\rho^I(t) = i\mathcal{U}^\dagger(t)\mathcal{V}\mathcal{U}(t)\rho^I(t)E(t) = i\mathcal{V}(t)\rho^I(t)E(t). \tag{1.7}$$

Here, the dipole operator $\mathcal{V}(t) = \mathcal{V}^I(t) = \mathcal{U}^\dagger(t)\mathcal{V}\mathcal{U}(t)$. The equation (1.7) or (1.6) will be our starting point for the following calculations.

1.2 Experimental setup, the order of nonlinearity

In the 2D spectroscopy, the nonlinear response of the molecular complex is detected. As the second order polarization $P^{(2)}$ vanishes for symmetry reasons [13], the lowest order polarization is $P^{(3)}$, third order polarization. In the experimental setup, we therefore mix together three pulses giving rise to the signal from linear and nonlinear polarization. The required nonlinear polarization is selected by non-collinear geometry of the incoming pulses by means of phase matching [13]. For the geometry of the pulses, see Fig. 1.1a.

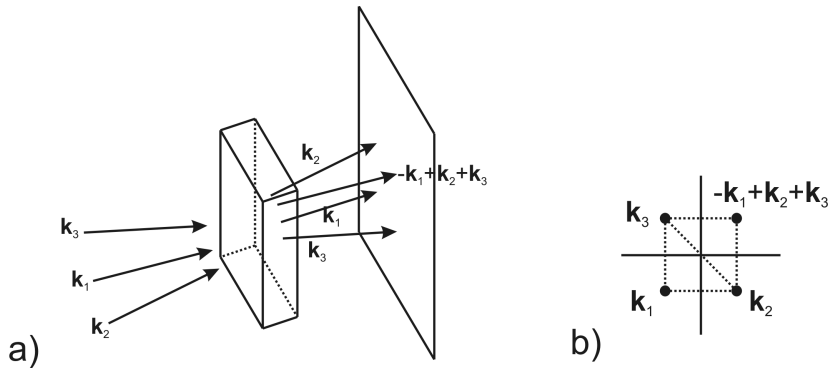

Figure 1.1: Four wave mixing experimental setup, phase matching geometry

The three pulses with wave vectors $\mathbf{k}_1$, $\mathbf{k}_2$, $\mathbf{k_3}$ mix in the sample, giving rise to the signal in different directions $\pm\mathbf{k}_1 \pm \mathbf{k}_2 \pm \mathbf{k}_3$. Behind the sample there are electric fields from the former three pulses and the signal present. To detect only the signal field, it is convenient to use a box-CARS (Coherent Anti-Stokes Raman Scattering) geometry, where the three incoming pulses intercept in the sample and then they form an equilateral triangle in the plane perpendicular to the propagation, see Fig. 1.1b. If we consider a signal in the direction $-\mathbf{k}_1+\mathbf{k}_2+\mathbf{k}_3$ it is then spatially separated from the incoming pulses and it can be easily resolved.

Homodyne or heterodyne detection of the signal can be used. In homodyne detection the intensity of the signal is detected. In heterodyne detection the signal is mixed with a weak so-called local oscilator field, enabling the detection of the intensity and also the phase.

All three incoming pulses must have well defined relative phases. The pulse ordering can be seen in Fig. 1.2.

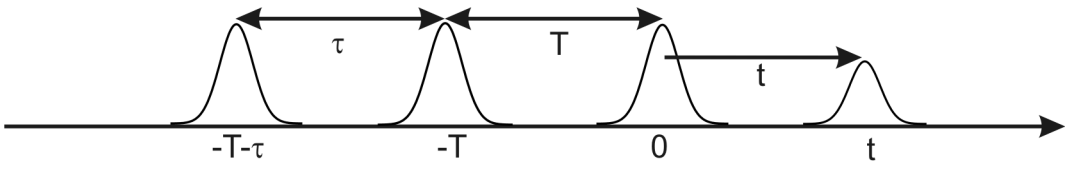

Figure 1.2: Pulse ordering

The incident electrical field consists of three pulses centered at $t = -\tau - T$, $t = -T$ and $t = 0$:

$$\mathcal{E}(t) = A(t+T+\tau)e^{i\mathbf{k}_1\cdot\mathbf{r}-i\omega(t+T+\tau)}+A(t+T)e^{i\mathbf{k}_2\cdot\mathbf{r}-i\omega(t+T)}+A(t)e^{i\mathbf{k}_3\cdot\mathbf{r}-i\omega t}+c.c. \quad (1.8)$$

Here, $A(t)$ is a slowly varying amplitude, $\mathbf{k}_i$ are the wave vectors of the pulses and ω is the carrier frequency (c.c. denotes complex conjugate). Often in this text we will use

$$E(t) = A(t+T+\tau)e^{i\mathbf{k}_1\cdot\mathbf{r}-i\omega(T+\tau)} + A(t+T)e^{i\mathbf{k}_2\cdot\mathbf{r}-i\omega T} + A(t)e^{i\mathbf{k}_3\cdot\mathbf{r}}. \quad (1.9)$$

The physical laser field is then

$$\mathcal{E}(t) = E(t)e^{-i\omega t} + E^*(t)e^{i\omega t}. \tag{1.10}$$

This arrangement is general and it covers several variants of the experimental setup. If we have $\mathbf{k}_1 = \mathbf{k}_2 \neq \mathbf{k}_3$, there are effectively 2 pulses interacting with the sample and using homodyne detection we have pump-probe spectroscopy. If we use different wave vectors and set $\tau = 0$, the first two pulses form a transient grating on which the third pulse is diffracted. And if we use pulses with different wave vectors, scan τ and use heterodyne detection, we have 2D spectroscopy.

1.3 Approximations used

Because in this thesis we are interested in the method of calculating the spectra in general, several approximations were used in order to make things more transparent. In many physical situations these approximations, however, prove to be perfectly applicable. In this section, the approximations are listed and described.

Dipole approximation, Condon approximation

Because the wavelength of the incident light is typically much larger than the characteristic size of the studied system, we can consider an interaction of the system with external (not quantized) electrical field in the form

$$H_{int} = -\boldsymbol{\mu} \cdot \mathbf{E}(t), \tag{1.11}$$

where $\boldsymbol{\mu}$ is a dipole moment operator. The dipole moments are considered being independent of the bath DOF.

System-bath interaction

The system-bath interaction is in general difficult to treat and some perturbation theory has to be used, usually in the second order of perturbation [11, 6, 1]. In order to include the system-bath interaction in the equations of motion for the RDM (1.6), the relaxation operator is introduced. It is a 4th rank tensor operator $\mathcal{R}_{ij,kl}$ responsible for the coherences dephasing and populations relaxation. In this thesis, in all calculations we choose the simplest form of system-bath interaction, which is a Redfield theory with secular approximation and a fast bath. Secular approximation means independent evolution of populations and coherences, $\mathcal{R}_{ij,kl} = 0$, $\omega_{ij} \neq \omega_{kl}$. Fast bath means Markovian approximation, which describes a bath with no memory. Redfield theory in this form leads to a simple exponential dephasing and population relaxation (no summation over indices here):

$$\frac{\partial \rho_{ij}}{\partial t}|_{diss} = -\Gamma_{ij}\rho_{ij}. \tag{1.12}$$

The lifetime of the coherences, $\tau_{ij} = \frac{1}{\Gamma_{ij}}$ leads to the homogeneous broadening of spectral peaks. It should be mentioned that an important purpose of 2D spectroscopy is to study the evolution of the peaks during the waiting time T. This dynamics is partially given by the system bath interaction. Therefore, when studying real molecules, more sophisticated model of system-bath interaction is usually used. When including the memory of the bath, additional difference between the perturbative and non-perturbative approach should arise. That is because in the equation of motion (1.6) for RDM there is no evolution of the bath. Integrating this equation in the non-perturbative approach, we then have no information of the bath state. In the perturbative approach, the memory of the bath is expressed in the form of bath correlation function leading, through the so-called cumulant expansion, to lineshape functions. Recently techniques were, however, developed to include the evolution of the bath into the equation of motion for the RDM by means of projection operators formalism [10, 14].

Rotating wave approximation (RWA)

Because the laser frequency ω and characteristic frequencies of the system corresponding to the energy level separation are of the same order of magnitude, we encounter terms where these frequencies subtract, yielding slowly oscillating terms, and terms where the frequencies add, resulting in rapidly oscillating terms. When the response functions (see Section 1.4) or equations (see Section 1.5) are integrated, the contribution of the rapidly oscillating terms will be much smaller than the contribution from the slowly oscillating terms and it can therefore be neglected. For particular example and more detailed discussion see Section 1.4.2.

Disorder

In a typical sample there are many molecules. These molecules are usually randomly oriented and one should therefore average over the dipole moments orientation. Moreover, due to the effect of local environment, the molecules have some distribution of transition frequencies. The calculated signal should be averaged over this distribution, which leads to an inhomogeneous broadening of the spectral peaks, giving them more 'round' shape. Because we calculated only model systems for sake of the calculation methods comparison and including the disorder would only result in larger computational time, we did neither of these averagings.

1.4 Perturbative approach

In this section, the perturbative language is used to calculate and describe the 2D spectrum. The idea of the perturbative approach is to express the reduced density matrix perturbatively in the order of the electric field and then select the desired order making use of (1.3):

$$P^{(3)}(t) = Tr\{\mu\rho^{(3)}(t)\}. \tag{1.13}$$

.

Solving the (1.7) iteratively (formally integrating, plugging it into itself), we get for the third order iteration

$$\rho^{I(3)}(t) \;=\; i^3 \int_{t_0}^{t} d\tau \int_{t_0}^{\tau} d\tau' \int_{t_0}^{\tau'} d\tau'' \mathcal{V}(\tau)\mathcal{V}(\tau')\mathcal{V}(\tau'')\rho^I(t_0)E(\tau)E(\tau')E(\tau''). \tag{1.14}$$

Now let us switch back from interaction picture $\rho^{(3)}(t) = \mathcal{U}(t)\rho^{I(3)}(t)$. Expressing $\mathcal{V}(t)$ in terms of propagators and using (1.13) we get for the polarization

$$\begin{gathered} P^{(3)}(t) = i^3 \textstyle\int_{t_0}^{t} d\tau \int_{t_0}^{\tau} d\tau' \int_{t_0}^{\tau'} d\tau'' \\ \times Tr\{\mu\mathcal{U}(t-\tau)\mathcal{V}\mathcal{U}(\tau-\tau')\mathcal{V}\mathcal{U}(\tau'-\tau'')\mathcal{V}\mathcal{U}(\tau'')\rho(t_0)\}E(\tau)E(\tau')E(\tau''). \end{gathered} \tag{1.15}$$

Finally, making the substitution $t_1 = \tau' - \tau''$, $t_2 = \tau - \tau'$, $t_3 = t - \tau$ and assuming the system is originally in equilibrium $\rho(t_0) = \rho(-\infty) = \rho_{eq}$, we get the polarization

$$\begin{aligned} P^{(3)}(t) = i^3 \int_0^\infty \int_0^\infty \int_0^\infty dt_1 dt_2 dt_3 Tr\{\mu\mathcal{U}(t_3)\mathcal{V}\mathcal{U}(t_2)\mathcal{V}\mathcal{U}(t_1)\mathcal{V}\rho_{eq}\} \\ \times E(t-t_3)E(t-t_3-t_2)E(t-t_3-t_2-t_1), \end{aligned} \tag{1.16}$$

$$\begin{aligned} P^{(3)}(t) = \int_{-\infty}^\infty \int_{-\infty}^\infty \int_{-\infty}^\infty dt_1 dt_2 dt_3 \times \\ S^{(3)}(t_3,t_2,t_1)E(t-t_3)E(t-t_3-t_2)E(t-t_3-t_2-t_1). \end{aligned} \tag{1.17}$$

Here, we defined the 3rd order response function

$$S^{(3)}(t_3,t_2,t_1) = i^3\theta(t_3)\theta(t_2)\theta(t_1)Tr\{\mu\mathcal{U}(t_3)\mathcal{V}\mathcal{U}(t_2)\mathcal{V}\mathcal{U}(t_1)\mathcal{V}\rho_{eq}\}. \tag{1.18}$$

In this definition $\theta(t)$ is the Heaviside theta (or step) function, which is equal to one for positive argument and vanishes for $t < 0$. It ensures the time ordering of interactions with the pulses. As one can see from Eq. (1.4), the polarization is basically a convolution the electric field at times $t = t_3$, $t = t_3 + t_2$ and $t = t_3 + t_2 + t_1$ with the response function of the molecule. Sometimes, the response functions are defined without the i^3 factor.

Now, we must insert the electric field (1.9) into (1.17). But before we do so, let us look on the evolution of the density matrix in the Liouville space.

1.4.1 Liouville space pathways

The Liouville space is a linear vector space with basis $|i\rangle\langle j|$, where $|i\rangle$ are the eigenstates of the molecular Hamiltonian. Each element of the basis thus corresponds to an element of the density matrix, and the density matrix is then a vector in the Liouville space. Evaluating the time evolution of the RDM in the response function (1.18), we obtain various terms, each corresponding to the dipole moment operator acting from the right or left in the commutators. These terms are called Liouville pathways, because each interaction with the dipole moment operator changes the element of the density matrix which evolves for the next time interval. Thus, every combination of μ corresponds to different sequence of states in the Liouville space. We start at the equilibrium state $|g\rangle\langle g|$ lying on the diagonal. In the end, we make the trace over the density matrix, which requires us to end on the diagonal as well. That is why only some of the pathways yield non-zero contribution. This set of pathways is given by the molecule band structure. The Liouville pathways are often conveniently expressed in terms of double sided Feynman diagrams [13, 6]. These diagrams show the elements of the density matrix as well as interactions with the pulses. An example of such a diagram is in Figure 1.3.

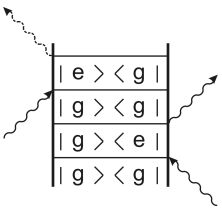

Figure 1.3: A Feynman diagram example. Its response function is, according to the rules described below, $R = \mu_{ge}\mathcal{U}_{eg}(t_3)(\frac{i}{\hbar}\mu_{eg})\mathcal{U}_{gg}(t_2)(\frac{i}{\hbar}\mu_{eg})\mathcal{U}_{ge}(t_1)(-\frac{i}{\hbar}\mu_{ge})\rho_{gg}$.

When properly read, the double-sided Feynman diagrams can be used to infer the response function of corresponding Liouville space pathway. The bra and ket vectors represent elements of the density matrix. Time flows upwards and the curly arrows represent interaction with the external electrical field. According to (1.7), each incoming arrow on the left multiplies the pathway by $\frac{i}{\hbar}\mu$ and each outgoing arrow on the left multiplies the pathway by $-\frac{i}{\hbar}\mu$. The right side is then a complex conjugate of the left side. Here, μ is a corresponding element of the dipole moment operator acting from the left or from the right. The last, dashed

curly arrow represents an emission of a signal field, which means multiplication by μ and taking the trace according to Eq. (1.13). Every horizontal line represents a change in the density matrix element and between them there is a free propagation of corresponding matrix elements. This propagator of ρ_{ij} element is a solution of a free equation of motion $\frac{\partial \mathcal{U}_{ij}}{\partial t} = -i\mathcal{L}_0\mathcal{U}_{ij}$ and has an oscillating phase factor $\sim e^{i\omega_{ij}t}$, where $\omega_{ij} = {}^{(\varepsilon_i-\varepsilon_j)}/_{\hbar}$ is a transition frequency between i-th and j-th energetic level of the molecule. From the double-sided Feynman diagram it is therefore immediately possible to read off the overall time phase factor of corresponding Liouville pathway. Inspecting these phase factors, we find that they can roughly be $S_R \sim e^{-i\Omega(t_3-t_1)}$, $S_{NR}e^{-i\Omega(t_3+t_1)}$ or $S_{DC} \sim e^{-i\Omega(t_3+2t_2+t_1)}$ where Ω is a typical transition frequency of the molecule. Generally (see for example Appendix B.2) the oscillation frequencies can be different for individual time intervals, but they are of the same magnitude. The terms are called rephasing, non-rephasing and double coherence, respectively. Rephasing because during t_3 the phase rotates in opposite direction than during t_1 and the phase is then regained. Double coherence because they have a two-exciton coherent state propagating during t_2 [6]. The time intervals between interactions correspond to time variables t_1, t_2, t_3 in (1.17). The response function corresponding to the given diagram is finally obtained multiplying the appropriate terms in the order bottom-up, see Fig. 1.3. The polarization is then calculated by integrating the response function multiplied by the electric field, see the next section. It turns out that the rephasing pathways have the pulse with $\mathbf{k}_1$ interacting as the first ($\tau > 0$) and the non-rephasing as the second ($\tau < 0$). This distinction is therefore not artificial and can be experimentally realised.

1.4.2 Polarization

Let us now return to the integration of (1.17). Inserting the external electric field (1.9), we get $6^3 = 216$ terms corresponding to 216 Liouville pathways to integrate, see previous Section 1.4.1. However, using non-collinear geometry we detect only the signal in the direction $-\mathbf{k}_1 + \mathbf{k}_2 + \mathbf{k}_3$**,** leaving just 6 terms with this spatial phase factor. They have a common time phase factor $e^{-i\omega(t-\tau)}$ and one of the phase factors $e^{i\omega(t_3-t_1)}$, $e^{i\omega(t_3+t_1)}$ or $e^{i\omega(t_3+2t_2+t_1)}$ under the integration. In order to proceed to the evaluation of the integral (1.17), we have to know the explicit form of the response function. As was shown in Section (1.4.1), it consists of several terms corresponding to the Liouville pathways with phase factors $e^{-i\Omega(t_3-t_1)}$, $e^{-i\Omega(t_3+t_1)}$ or $e^{-i\Omega(t_3+2t_2+t_1)}$. Assuming Ω is similar to the laser carrier frequency ω, we obtain terms where the oscillating factors cancel with the factors from the electrical field, giving $e^{-i(\Omega-\omega)(t_3-t_1)}$ etc. and terms where the frequencies add. The slowly oscillating terms will have much larger contribution to the integral than the rapidly oscillating ones. We can therefore employ RWA, see Section 1.3, neglecting the rapidly oscillating terms. Denoting the pathways from response function with different phase factors as $S_R^{(3)}$, $S_{NR}^{(3)}$ and $S_{DC}^{(3)}$, we arrive at

$$
\begin{aligned}
P^{(3)}(t,T,\tau) = e^{-i\omega(t-\tau)} \int_{-\infty}^{\infty}\int_{-\infty}^{\infty}\int_{-\infty}^{\infty} dt_1 dt_2 dt_3 \times \\
\{S_R^{(3)}(t_3,t_2,t_1)[A(t+T-t_3)A(t-t_3-t_2)A^*(t+T+\tau-t_3-t_2-t_1) \\
+A(t-t_3)A(t+T-t_3-t_2)A^*(t+T+\tau-t_3-t_2-t_1)]e^{i\omega(t_3-t_1)} \\
+S_{NR}^{(3)}(t_3,t_2,t_1)[A(t+T-t_3)A^*(t+T+\tau-t_3-t_2)A(t-t_3-t_2-t_1) \\
+A(t-t_3)A^*(t+T+\tau-t_3-t_2)A(t+T-t_3-t_2-t_1)]e^{i\omega(t_3+t_1)} \\
+S_{DC}^{(3)}(t_3,t_2,t_1)[A^*(t+T+\tau-t_3)A(t+T-t_3-t_2)A(t-t_3-t_2-t_1) \\
+A^*(t+T+\tau-t_3)A(t-t_3-t_2)A(t+T-t_3-t_2-t_1)]e^{i\omega(t_3+2t_2+t_1)}\}.
\end{aligned}
\tag{1.19}
$$

To calculate the third order polarization, it is therefore necessary to evaluate this integral.

It is worth noting that for even orders of polarization, the response functions oscillate with a time phase factor $\sim e^{-ik2\Omega t}$, $k \in \mathbb{N}_0$. This can be seen from the double sided Feynman diagrams, see Section 1.4.1, which include even number of interactions. This fact means that they do not survive the RWA. When employing the RWA, only the odd orders of polarization are non-vanishing.

1.5 Non-perturbative approach

1.5.1 The equations of motion

In the non-perturbative approach we start with known initial conditions such as $\rho(t_0) = \rho_{eq} = |g\rangle\langle g|$. We use explicit form of μ and $\mathcal{R}$ according to the calculated system and the external field (1.9). Optionally, we can apply RWA in the form of an ansatz $\rho_{kl} = \sigma_{kl}e^{-i(k-l)\omega t}$ or similar, and keep only the slowly oscillating terms. This not only simplifies the problem but results in better stability of the computation by eliminating the rapidly oscillating terms. Then, we numerically solve the (coupled) set of equations for the density matrix (1.6). Finally, we multiply by μ and take the trace to obtain the polarization. After that, we obtain the complex polarization including the polarization of all non-vanishing orders in all possible directions. The next step is therefore subtracting the linear polarization from the three pulses. For this, we have to compute the equations three more times, once for each pulse. Finally, we have to extract the polarization in the required direction, in our case $-\mathbf{k}_1 + \mathbf{k}_2 + \mathbf{k}_3$. This process is called phase cycling.

1.5.2 Phase cycling

Since we calculate the response of one molecule, let us denote the phase of the pulses as $\Phi_i = \mathbf{k}_i \cdot \mathbf{r}$. Considering the triple action of the dipole moment operator on the density matrix when interacting from the left and from the right, see (1.4.1), one can deduce [8] that the overall third order polarization will have phase

$$P^{(3)} \sim e^{in_1(\Phi_3-\Phi_1)+in_2(\Phi_3-\Phi_2)+i\Phi_3}, \tag{1.20}$$

where n_1, $n_2 \in \{-2,-1,0,1\}$ and $n_1+n_2 \in \{-2,-1,0,1\}$. There are 12 different pairs of n_1, n_2 fulfilling these conditions, giving rise to polarization in 12 different directions. Since the polarization phase depends only on the difference between phases, let us denote $\delta_1 = \Phi_3 - \Phi_1$, $\delta_2 = \Phi_2 - \Phi_1$. For convenience, we will set $\Phi_3 = 0$ for now (we can always return to it later, but for our calculation the overall phase is irrelevant). The calculated third order polarization then depends on the relative phase differences between the pulses δ_1, δ_2, and it is the sum of the polarizations in all possible directions:

$$P^{(3)}(\delta_1,\delta_2) = \sum_{n_1,n_2} P_{n_1n_2} e^{in_1\delta_1+in_2\delta_2}. \tag{1.21}$$

Clearly, the desired polarization component in the direction $-\mathbf{k}_1+\mathbf{k}_2+\mathbf{k}_3$ is the one with $n_1 = 1$, $n_2 = -1$, P_{1-1}. Now, by plugging different phases into (1.21), we can generate equations for the polarization components. When we have 12 of them, we can write it as a set of equations (index $^{(3)}$ is omitted here)

$$\begin{pmatrix} P(0,0) \\ P(\pi/2,0) \\ P(\pi,0) \\ P(3\pi/2,0) \\ P(0,\pi/2) \\ P(\pi,\pi/2) \\ P(3\pi/2,\pi/2) \\ P(0,\pi) \\ P(0,3\pi/2) \\ P(\pi/2,\pi) \\ P(\pi,\pi) \\ P(\pi/2,\pi/2) \end{pmatrix} = \mathcal{M} \begin{pmatrix} P_{-20} \\ P_{-21} \\ P_{-1-1} \\ P_{-10} \\ P_{-11} \\ P_{0-2} \\ P_{0-1} \\ P_{00} \\ P_{01} \\ P_{1-2} \\ P_{1-1} \\ P_{10} \end{pmatrix}, \tag{1.22}$$

where

$$\mathcal{M} = \begin{pmatrix} 1 & 1 & 1 & 1 & 1 & 1 & 1 & 1 & 1 & 1 & 1 & 1 \\ -1 & -1 & -i & -i & -i & 1 & 1 & 1 & 1 & i & i & i \\ 1 & 1 & -1 & -1 & -1 & 1 & 1 & 1 & 1 & -1 & -1 & -1 \\ -1 & -1 & i & i & i & 1 & 1 & 1 & 1 & -i & -i & -i \\ 1 & i & -i & 1 & i & -1 & -i & 1 & i & -1 & -i & 1 \\ 1 & i & i & -1 & -i & -1 & -i & 1 & i & 1 & i & -1 \\ -1 & -i & 1 & i & -1 & -1 & -i & 1 & i & i & -1 & -i \\ 1 & -1 & -1 & 1 & -1 & 1 & -1 & 1 & -1 & 1 & -1 & 1 \\ 1 & -i & i & 1 & -i & -1 & i & 1 & -i & -1 & i & 1 \\ -1 & 1 & i & -i & i & 1 & -1 & 1 & -1 & i & -i & i \\ 1 & -1 & 1 & -1 & 1 & 1 & -1 & 1 & -1 & -1 & 1 & -1 \\ -1 & -i & -1 & -i & 1 & -1 & -i & 1 & i & -i & 1 & i \end{pmatrix}. \quad (1.23)$$

Solving this set of equations by inverting $\mathcal{M}$, we get for the required polarization

$$\begin{aligned} P_{1-1} = \frac{1}{8}\{&2P(0,0) - (1+i)P(0,\pi) - (1-i)P(0,{}^{\pi}/_{2}) \\ &+(1-i)P(\pi,\pi) - (1-i)P(\pi,{}^{\pi}/_{2}) - (1+i)P({}^{\pi}/_{2},0) + 2iP({}^{\pi}/_{2},\pi) \\ &+(1-i)P({}^{\pi}/_{2},{}^{\pi}/_{2}) - (1-i)P({}^{3\pi}/_{2},0) + (1-i)P({}^{3\pi}/_{2},{}^{\pi}/_{2})\}. \end{aligned} \quad (1.24)$$

The procedure for calculation is thus as follows. For different phase factors of the pulses 10 density matrices must be propagated simultaneously in time (not necessarily 12, as used in [8]). Three more density matrices, one for each pulse, must be also propagated, giving the linear polarization. From each of the 10 density matrices the polarization is calculated, then the linear polarizations are subtracted. Finally, the polarization component in a the required direction is extracted according to (1.24). By this, we get the third required order polarization in given direction and also all non-vanishing higher order polarizations. In experiment, this phase cycling is done automatically by individual molecules in the sample feeling different phases. Apart from this natural phase cycling an experimental phase cycling can be used. Here, by using sequences of pulses with defined phase differences it is possible to select desired pathways, remove unwanted scattering etc. For more details see for example [6].

Different method using even smaller number of density matrices (for 2D spectrum seven are required) propagating in time was developed by Gelin *et al.*[5]. This method combines the perturbative approach with density matrix propagation schemes, and it is therefore excluding higher order polarization contributions. Since it is less transparent and straightforward, it is not used in this thesis. For more complicated systems it could, however, prove to be useful by saving computational time and by restricting the calculation only to the third order of polarization.

1.6 2D Spectrum

Having the time-dependent third order signal field $E_S(t, T, \tau)$ for given pulse times T and τ , to obtain a 2D spectrum one performs two-dimensional Fourier transform in t and τ. Why these two variables can be seen by analogy with a linear (first order) response:

$$\begin{aligned} P^{(1)}(t) &= \left(\frac{i}{\hbar}\right) \int_0^\infty dt_1 Tr\{\mu \mathcal{U}(t_1)\mathcal{V}\rho_{eq}\}E(t-t_1) \\ &= \int_0^\infty dt_1 S(t_1)E(t-t_1). \end{aligned} \tag{1.25}$$

Where $S(t_1)$ is the first order response function defined by the formula. Performing Fourier transform of this convolution, bearing in mind that Eq. (1.4) and the relation $\mathcal{F}(f * g) = \mathcal{F}(f)\mathcal{F}(g)$, we get

$$E_S(\omega) = iP^{(1)}(\omega) = iS(\omega)E(\omega) = \varepsilon_0\chi(\omega)E(\omega). \tag{1.26}$$

This means that i times the Fourier transform of the response function can be identified with susceptibility times ε_0, $iS(\omega) \sim \varepsilon_0\chi(\omega)$. This implies the absorption coefficient α is proportional to its real part [13]:

$$\alpha(\omega) \sim Re\{S(\omega)\}. \tag{1.27}$$

When we look at the beginning, we see that the part $\mu\mathcal{U}(t)\mathcal{V}\rho$ corresponds to the absorptive part. Comparing this with (1.18), we see that we have this term here twice: first it acts directly on the equilibrium density matrix ρ_{gg}, hence the transform in the third argument, then it acts on the density matrix after the first two interactions and evolution during t_2, hence the transform in the first argument. For the third order response the absorptive spectrum is obtained by summing of the rephasing and non-rephasing parts and taking the real part [6]. As mentioned in Section 1.4.1, the rephasing pathways correspond to $\tau > 0$, while the non-rephasing correspond to $\tau < 0$. To obtain positive frequency ω_τ, we have to Fourier transform the rephasing and non-rephasing part with a different sign in τ:

$$S(\omega_t, T, \omega_\tau) = \int_{-\infty}^{\infty} dt \int_{-\infty}^{\infty} d\tau \, (S_R(t, T, \tau)e^{-i\omega_\tau\tau} + S_{NR}(t, T, \tau)e^{i\omega_\tau\tau})e^{i\omega_t t}. \tag{1.28}$$

When we want the absorptive spectrum, we take the real part of $S(\omega_t, T, \omega_\tau)$.

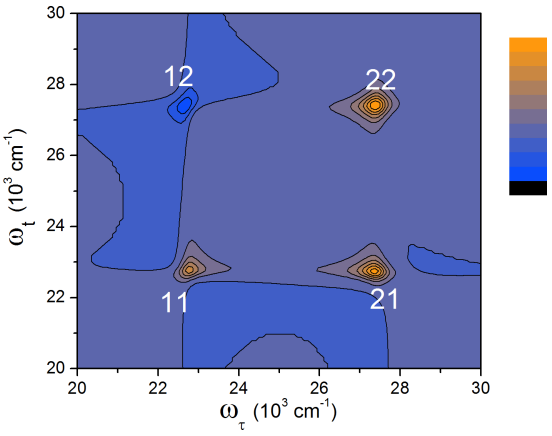

Figure 1.4: An example of a 2D spectrum. The excitation frequency is on the horizontal axis, the emission frequency on the vertical axis. The numbers denote the peaks, first number means excitation frequency and the second emission frequency. Being a spectrum of a three-band system, only two characteristic frequencies are present. The blue colour means negative values, the orange positive values, see relative scale. The contours are plotted in 10% of the overall range (from min. to max. value) intervals.

An example of such a spectrum is in Figure 1.4. This is an absorptive spectrum of a coupled dimer for waiting time $T = 160$ fs, see Section 2.2. All 2D spectra in this thesis will follow the same plotting convention. As we can see, there are several peaks present, their notation is described below the Figure. The peaks 11 and 22 are for obvious reason called diagonal, the peaks 21 and 12 are called off-diagonal. When describing energy transfer, the off diagonal peaks are usually of interest, because they represent absorption followed by an emission at different frequency.

2. Computer simulation

In this chapter, the 2D spectra of a two-level system and a coupled dimer are calculated using both perturbative and non-perturbative approaches. For each system a brief description is given and the resulting spectra are compared. The numerical implementation of the approaches is also described. The parameters of the systems are chosen to resemble realistic molecules.

2.1 Two-level system

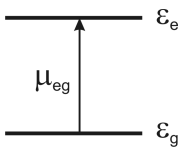

Figure 2.1: A scheme of a two-level system energy levels

The simplest system to study is a molecule with two energy levels - ground state and excited state, see Figure 2.1. The system Hamiltonian in excitonic basis is

$$H_S = |g\rangle \varepsilon_g \langle g| + |e\rangle \varepsilon_e \langle e| , \tag{2.1}$$

where g and e denote the ground and excited state and ε_i is the energy of state i. The transition dipole operator in the same basis reads

$$\mu = |g\rangle \mu_{ge} \langle e| + |e\rangle \mu_{eg} \langle g| . \tag{2.2}$$

2.1.1 Perturbative approach

The possible Liouville pathways are illustrated in Fig. 2.2 as Feynman diagrams. From here, we can infer the form of the response functions. As can be easily derived [13], the free propagator of ρ_{ij} can we written as

$$\mathcal{U}_{ij}(t) = e^{-i\omega_{ij}t - \Gamma_{ij}t}, \; i,j \in \{e,g\}. \tag{2.3}$$

Here $\omega_{ij} = \frac{\varepsilon_i - \varepsilon_j}{\hbar}$ (this can be seen from the definition of $\mathcal{U}$: $\mathcal{U}(t)\bullet = U^\dagger(t) \bullet U(t)$ and $U_i(t) = e^{-\frac{i}{\hbar}\varepsilon_i t}$) and $\Gamma_{ij} = \Gamma_{ji}$ is dephasing (coherence for $i \neq j$ and population for $i = j$) coming from the Redfield theory, here included phenomenologically. Because the population relaxation Γ_{ii} is typically much slower than coherence dephasing, it will be neglected on considered time scale.

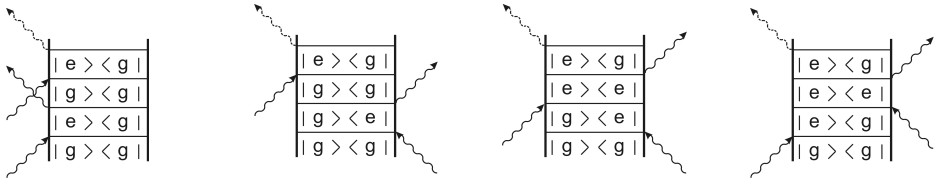

Figure 2.2: The possible Liouville space pathways for a two-level system. Left to right: R_1, R_2, R_3, R_4

Furthermore, each interaction with the field adds factor $\frac{i}{\hbar}\mu_{eg}e^{i\Phi}$ or its complex conjugate, according to the rules explained in Section 1.4.1. Knowing this, we can readily write the expressions for individual pathways:

$$R_1(t_3,t_2,t_1) = (\frac{i}{\hbar})^3|\mu_{eg}|^4 e^{-i\omega_{eg}(t_3+t_1)}e^{-\Gamma(t_3+t_1)}, \tag{2.4}$$

$$R_2(t_3,t_2,t_1) = (\frac{i}{\hbar})^3|\mu_{eg}|^4 e^{-i\omega_{eg}(t_3-t_1)}e^{-\Gamma(t_3+t_1)}, \tag{2.5}$$

$$R_3(t_3,t_2,t_1) = (\frac{i}{\hbar})^3|\mu_{eg}|^4 e^{-i\omega_{eg}(t_3-t_1)}e^{-\Gamma(t_3+t_1)}, \tag{2.6}$$

$$R_4(t_3,t_2,t_1) = (\frac{i}{\hbar})^3|\mu_{eg}|^4 e^{-i\omega_{eg}(t_3+t_1)}e^{-\Gamma(t_3+t_1)}. \tag{2.7}$$

Here, we denote coherence dephasing $\Gamma_{eg} = \Gamma_{ge} = \Gamma$. According to Eq. (1.19) , we can write

$$\begin{aligned} P^{(3)}(t,T,\tau) = e^{-i\omega(t-\tau)}\textstyle\int_0^\infty\int_0^\infty\int_0^\infty dt_1dt_2dt_3\,\{[R_2(t_3,t_2,t_1)+R_3(t_3,t_2,t_1)]\times \\ [A(t+T-t_3)A(t-t_3-t_2)A^*(t+T+\tau-t_3-t_2-t_1) \\ +A(t-t_3)A(t+T-t_3-t_2)A^*(t+T+\tau-t_3-t_2-t_1)]e^{i\omega(t_3-t_1)} \\ +[R_1(t_3,t_2,t_1)+R_4(t_3,t_2,t_1)]\times \\ [A(t+T-t_3)A^*(t+T+\tau-t_3-t_2)A(t-t_3-t_2-t_1)+ \\ A(t-t_3)A^*(t+T+\tau-t_3-t_2)A(t+T-t_3-t_2-t_1)]e^{i\omega(t_3+t_1)}\}. \end{aligned} \tag{2.8}$$

To get some intuitive physical insight, let us consider an ultra-short pulses limit. This means the envelope of the pulse is represented by delta function $A(t) = \delta(t)$. (for simplicity we assume unit amplitude of the field). The electric field (1.9) then becomes

$$E(t) = \delta(t+T+\tau)e^{i\mathbf{k}_1\cdot\mathbf{r}-i\omega(t+T+\tau)} + \delta(t+T)e^{i\mathbf{k}_2\cdot\mathbf{r}-i\omega(t+T)}\delta(t)e^{i\mathbf{k}_3\cdot\mathbf{r}-i\omega t}, \tag{2.9}$$

representing 3 sharp pulses in fixed times $t = -T-\tau$, $t = -T$, and $t = 0$.

A little care is needed here since we applied the RWA first and then introduced the delta-shape pulses, still expecting the rapidly oscillating terms to cancel. This is called a physical delta function, meaning the pulses are so short in comparison

with other relevant timescales such as the decoherence time or time scanning range, that they can be mathematically represented by delta function, but in the integration we still neglect the rapidly oscillating terms.

The delta functions cancel the integration and since the integration times t_3, t_2, t_1 are positive ensuring causality, only some terms survive. For the rephasing part it is the term with $t_3 = t$,$t_2 = T$, $t_1 = \tau$, meaning the pulse ordering $-k_1$, k_2, k_3 and for the non-rephasing part $t_3 = t$, $t_2 = T + \tau$, $t_1 = -\tau$, being non-zero only for negative τ, which means pulse ordering k_2, $-k_1$, k_3. Here, we make substitution $\tau \to -\tau$ and realizing that T now no longer means the waiting time (the time between the second and third pulse, during which the population evolves), we also substitute $T \to T + \tau$. So, finally, we have for positive τ and waiting time T polarization

$$P^{(3)}(t, T, \tau) = \theta(t)\theta(T)\theta(\tau)(\frac{i}{\hbar})^3|\mu_{eg}|^4 2[e^{-i\omega_{eg}(t-\tau)} + e^{-i\omega_{eg}(t+\tau)}]e^{-\Gamma(t+\tau)}, \quad (2.10)$$

where the first term in the square brackets is the rephasing part and the second term is the non-rephasing part. Here, it is also easy to see why they are called rephasing and non-rephasing, because for fixed τ in the former the phase is at time $t = \tau$ regained (and, when inhomogeneous broadening is included as some transition frequencies distribution, photon echo appears [8]), while in the latter the phase still grows. The signal field is obtained by multiplying by i in accordance with (1.4):

$$E_S(t, T, \tau) = \theta(t)\theta(T)\theta(\tau)(\frac{1}{\hbar})^3|\mu_{eg}|^4 2[e^{-i\omega_{eg}(t-\tau)} + e^{-i\omega_{eg}(t+\tau)}]e^{-\Gamma(t+\tau)}. \quad (2.11)$$

2.1.2 Non-perturbative approach

Let us use the electric field in the form (1.9) and use RWA ansatz $\rho_{eg} = \sigma_{eg}e^{-i\omega t}$ [8]. Neglecting the terms oscillating more rapidly than $\sim e^{\pm i\omega t}$ and including system-bath interaction in the form of exponential dephasing, the equation (1.6) becomes

$$\frac{\partial \sigma_{eg}}{\partial t} = -i(\omega_{eg} - \omega)\sigma_{eg} - \Gamma\sigma_{eg} + \frac{i}{\hbar}\mu_{eg}E(t)(\rho_{gg} - \rho_{ee}), \quad (2.12)$$

$$\frac{\partial \rho_{gg}}{\partial t} = -\frac{i}{\hbar}\mu_{eg}\sigma_{ge}E(t) + \frac{i}{\hbar}\mu_{ge}\sigma_{eg}E^*(t), \quad (2.13)$$

$$\frac{\partial \rho_{ee}}{\partial t} = +\frac{i}{\hbar}\mu_{eg}\sigma_{ge}E(t) - \frac{i}{\hbar}\mu_{ge}\sigma_{eg}E^*(t). \quad (2.14)$$

which are the celebrated Bloch equations for reduced density matrix. Note that although the density matrix has four components, because of its Hermiticity

($\sigma_{ge} = \sigma_{eg}^{\star}$) we have only three independent equations. Here, Γ is a coherence dephasing rate. This form of dephasing comes from the Redfield theory described in Section 1.3.

Again, to get some intuitive physical insight, the ultra-short pulses limit will be investigated, see (2.9).

With the delta function form of $E(t)$, we are able to solve the equations analytically. The idea is that the delta function on the right hand side of a first order ordinary differential equation (ODE) represents an initial condition:

$$y'(t) + Ay(t) = C\delta(t - t_0). \tag{2.15}$$

This has a solution

$$y(t) = (y_- + C\theta(t - t_0))e^{At_0}e^{-At}, \tag{2.16}$$

where $y_- = \lim_{t \to t_0^-} y(t)$ is the value of y before the delta pulse comes and at $t = t_0$ y jumps by C and propagates freely afterwards.

For a detailed calculation see Appendix A.1. After solving Eqs. (2.12),(2.13) and (2.14) between the pulses, we finally arrive at

$$\sigma_{eg}^{\Phi}(t) = \theta(t)\theta(T)\theta(\tau)\frac{-i\mu_{eg}|\mu_{eg}|^2}{\hbar^3}2e^{-i\omega_{eg}(t-\tau)-\Gamma(t+\tau)}e^{i\omega t}, \tag{2.17}$$

where Φ means with the phase $e^{i(-\Phi_1+\Phi_2+\Phi_3)}$. Coming back from RWA $\rho_{eg} = \sigma_{eg}e^{-i\omega t}$ and using the fact that polarization corresponds to the expectation value of μ (1.13), we get the signal field

$$P_R^3 = -i\theta(t)\theta(T)\theta(\tau)\frac{|\mu_{eg}|^4}{\hbar^3}2e^{-i\omega_{eg}(t-\tau)-\Gamma(t+\tau)}. \tag{2.18}$$

Performing exactly the same procedure but for switched order of the first two pulses, we get

$$P_{NR}^3 = -i\theta(t)\theta(T)\theta(\tau)\frac{|\mu_{eg}|^4}{\hbar^3}2e^{-i\omega_{eg}(t+\tau)-\Gamma(t+\tau)}. \tag{2.19}$$

Finally, summing the two pulse orderings together and using (1.4), we get for the signal field

$$E_S(t, T, \tau) = \theta(t)\theta(T)\theta(\tau)\frac{|\mu_{eg}|^4}{\hbar^3}2(e^{-i\omega_{eg}(t-\tau)} + e^{-i\omega_{eg}(t+\tau)})e^{-\Gamma(t+\tau)}. \tag{2.20}$$

which is exactly the same as (2.20). This means that for the two-level system with described kind of relaxation and ultra-short pulses the perturbative and non-perturbative approaches are equivalent.

2.1.3 Comparison for finite pulses

Because we learnt that for infinitely (in the sense of the envelope) short pulses the perturbative and non-perturbative approach are equivalent, we must turn to a little more realistic setup. Let us therefore consider finite pulses. For the perturbative approach this means we have to actually evaluate the integral (2.8). For the non-perturbative approach we have to solve the Eqs. (2.12), (2.13) and (2.14) with pulses of finite length. As a realistic approximation a Gaussian profile of the pulses was chosen:

$$A(t) = E_0 \frac{1}{\sqrt{2\pi}d} e^{-t^2/2d^2}. \tag{2.21}$$

The evaluation of the triple integral was performed by simply using the trapezoidal rule integrating over the relevant time intervals corresponding to the position of the pulses. The integration interval was chosen as $(t_p - \varepsilon, t_p + \varepsilon)$, where t_p is the position of the pulse center for considered time variable and ε is chosen so the pulse is sufficiently small on the edges of the integration interval. This is achieved by enlarging ε and checking the difference in calculated signal. The integration step used was 1.5 fs.

For the integration of the equations of motion for the density matrix, the fourth order Runge-Kutta (RK) with constant time step 0.5 fs was used. The evaluation was tested for error by performing the same integration with smaller RK step and checking the difference in calculated signal.

The values of the two-level system parameters used for calculation are in Table 2.1.

Parameter	Value
$\mu_{eg} = \mu_{ge}$	1.0
coherence dephasing Γ	100 fs^{-1}
waiting time T	100 fs
$\omega = \omega_{eg}$	25 000 cm^{-1}, equivalent to $\lambda = 400$ nm
pulse width d	7 fs

Table 2.1: Parameters for two-level system

The parameters were set to represent a real molecule with one possible excited state. The transition frequency is in a typical range, for example Chlorophyll A has an absorption peak around 430 nm.

For both methods the signal was calculated in the range $t, \tau \in [0, 1200]$ fs and the polarization was outputted every 2 fs for both variables. The calculated time-dependent signal was further processed by two dimensional fast Fourier transform (FFT) using the FFTW library [4]. In t we use backward FT $\int_{-\infty}^{\infty} e^{i\omega_t t}$. In order to get positive frequencies, we use for non-rephasing part backward FT $\int_{-\infty}^{\infty} e^{i\omega_\tau \tau}$ and for rephasing part forward FT $\int_{-\infty}^{\infty} e^{-i\omega_\tau \tau}$ in τ, see Section 1.6 . For better resolution a zero padding of 1200 fs was used. The resulting 2D spectra are then depicted in form of contour plots in Fig. 2.3.

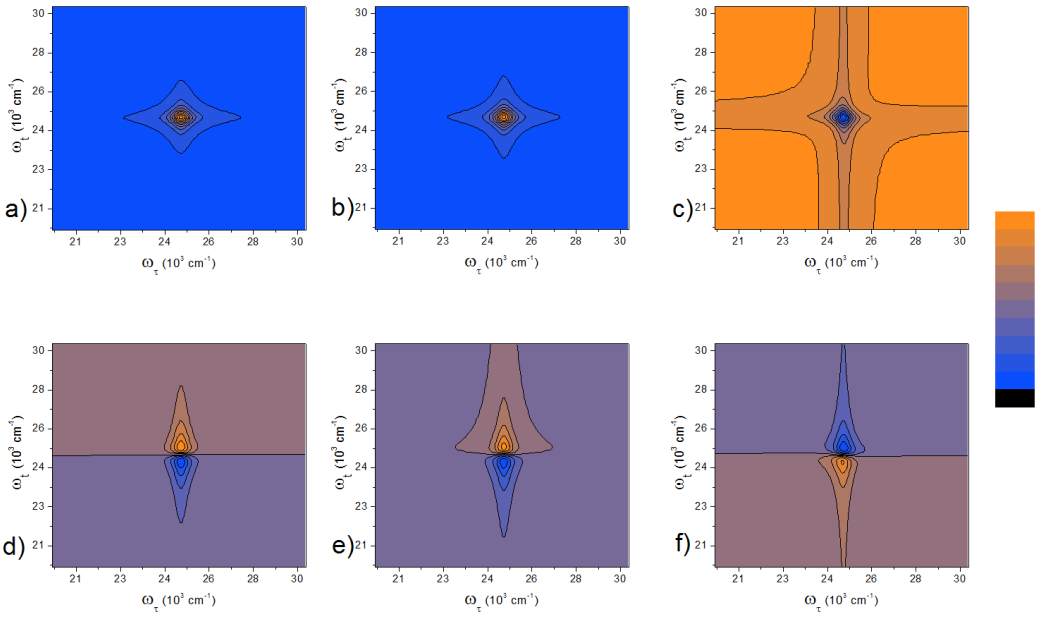

Figure 2.3: The 2D spectrum of a two-level system calculated non-perturbatively (first column a),d)) and perturbatively (second column b),e)). In the third column there are the previous two spectra subtracted (c), f)). The first row (a),b),c)) includes the real (absorptive) part of the spectrum and the second row (d),e),f)) includes the imaginary part of the spectrum.
The contours are plotted in 10% of the overall range (from min. to max. value) intervals, orange means positive and blue negative values, the scale is relative. The spectra were not rescaled.

As can be seen from Fig. 2.3, on the first sight the perturbatively and non-perturbatively calculated spectra look the same. Only after their subtraction the difference, which is approximately two orders of magnitude smaller, can be seen. Also, the difference looks like a former spectrum with inverted sign. Let us now explain this fact.

2.1.3.1 Fifth-order response model

When there is no memory of the path of the system in the Liouville space stored in the bath, the only difference between the perturbatively and non-perturbatively calculated spectrum is that the latter contains also a contribution of higher orders of nonlinearity. That is because in its calculation we calculated the overall polarization and then the linear part was subtracted, leaving the higher order contributions included. The fourth order response vanishes because of RWA, see Section1.4.2. Let us therefore calculate the fifth order response and see if it looks like the difference obtained.

For clarity and simplicity, we use 5 consequent δ-pulses as a model of 5 interactions. The time separations between them are τ, T, T_1, T_2 and the spectrum is taken in time t. Evaluating one particular pathway in the direction $-\mathbf{k}_1 + \mathbf{k}_2 + \mathbf{k}_3 - \mathbf{k}_3 + \mathbf{k}_3$ which is the same as $-\mathbf{k}_1 + \mathbf{k}_2 + \mathbf{k}_3$, we get the polarization dependence

$$P \sim (\frac{i}{\hbar})^5 e^{-i\omega_{eg}(t+T_2-\tau)-\Gamma(t+T_2+\tau)}. \tag{2.22}$$

Because it oscillates with the transition frequency ω_{eg} in three time variables, performing the Fourier transform we would get a 3D spectrum. Because we plot a 2D spectrum and have no control of the time T_2 (the interaction can occur at any time during the interaction with the 3rd pulse), we must integrate over the T_2. The interactions time-ordering and the Liouville pathway are in Figure 2.4

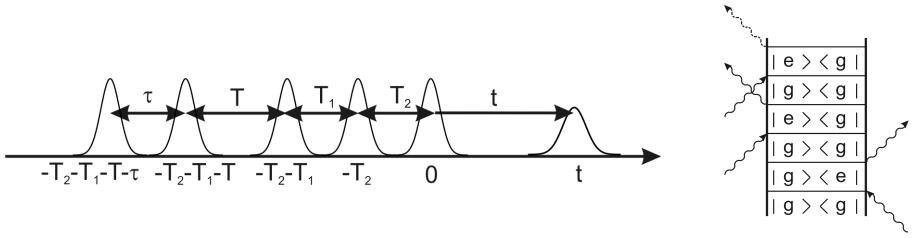

Figure 2.4: The pulse ordering for the 5th order response model and the considered Liouville space pathway.

Now, we try to fit this model on our three finite pulses. For the considered pathway, only one interaction with the first two pulses occured and we will therefore treat them as δ-pulses in times $-T_2 - T_1 - T - \tau$ and $-T_2 - T_1 - T$. With the third pulse there were three interactions present, hence we must treat it as finite and the fifth interaction which happens in time $-T_2$ could have happened in any time during the presence of the third pulse. Technically, this means we are to integrate over T_2 from 0 to infinity, taking into account the (Gaussian) envelope of the third pulse:

$$\begin{aligned} P &\sim (\frac{i}{\hbar})^5 e^{-i\omega_{eg}(t-\tau)-\Gamma(t+\tau)} \int_0^\infty e^{-i\omega_{eg}T_2-\Gamma T_2} \frac{1}{\sqrt{\pi}d} e^{-\frac{T_2^2}{d^2}}, \\ P &\sim -\frac{1}{2\hbar^2} e^{-(\omega_{eg}^2-\Gamma^2)\frac{d^2}{4}} e^{2i\omega_{eg}\Gamma\frac{d^2}{4}} (\frac{i}{\hbar})^3 e^{-i\omega_{eg}(t-\tau)-\Gamma(t+\tau)}, \end{aligned} \tag{2.23}$$

which is precisely the rephasing response function of the 3rd order (2.5) with a prefactor $-\frac{1}{2\hbar^2} e^{-(\omega_{eg}^2-\Gamma^2)\frac{d^2}{4}} e^{2i\omega_{eg}\Gamma\frac{d^2}{4}}$. Because the interaction with the third pulse can occur in any time, we also have to consider the pathway with interactions ordering $-\mathbf{k}_1 + \mathbf{k}_2 - \mathbf{k}_3 + \mathbf{k}_3 + \mathbf{k}_3$. This differs from the evaluated one only in the fact that it oscillates with $-\omega_{eg}$ during T_2, which gives a prefactor $-\frac{1}{2\hbar^2} e^{-(\omega_{eg}^2-\Gamma^2)\frac{d^2}{4}} e^{-2i\omega_{eg}\Gamma\frac{d^2}{4}}$ after integration. Summing these two pathways together, we then get a prefactor $-\frac{1}{\hbar^2} e^{-(\omega_{eg}^2-\Gamma^2)\frac{d^2}{4}} cos(2\omega_{eg}\Gamma\frac{d^2}{4})$. Switching the order

of the first two pulses changes nothing in the procedure of integration and gives us the non-rephasing part with the same prefactor. For fixed transition frequency ω_{eg} and pulse width d so small that $\frac{1}{2}\omega_{eg}\Gamma d^2 < \frac{\pi}{2}$, which is easily fulfilled in our calculations, see Table 2.1, this prefactor is a negative real number. This means that it produces the same spectrum, only with inverted sign, exactly as in Fig. 2.3.

2.1.3.2 Order of the spectrum

Another, more qualitative way to see which order of polarization we have is to test the dependence of the magnitude of the signal for a fixed point of the spectrum on the electrical field amplitude. Assuming that all three pulses have the same amplitude E_0 (see (2.21) and (1.9)), the perturbatively calculated signal should be proportional to E_0^3:

$$S_P = aE_0^3. \tag{2.24}$$

The non-perturbatively calculated response, on the other hand, includes contribution from all the unsubtracted higher order polarizations:

$$S_{NP} = aE_0^3 + bE_0^5 + ... \tag{2.25}$$

The perturbatively computed spectrum is, of course, proportional to E_0^3, because it is multiplied by it in the end. We can, nevertheless, test this dependence for the non-perturbatively calculated spectrum S_{NP}.

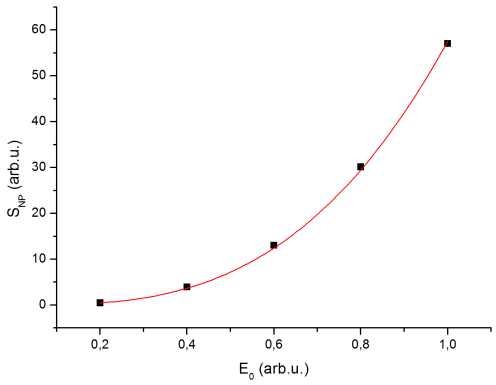

Figure 2.5: The dependence of non-perturbatively calculated signal amplitude on field amplitude. Black squares are calculated values, red line is a cubic function fit according to (2.24).

As can be seen from the Fig. 2.5, the signal goes, more or less, as E_0^3. Let us now explain the deviation from this dependence.

Subtracting S_P from S_{NP}, we get

$$S_{NP} - S_P = bE_0^5. \tag{2.26}$$

where we neglected the higher orders of polarization.

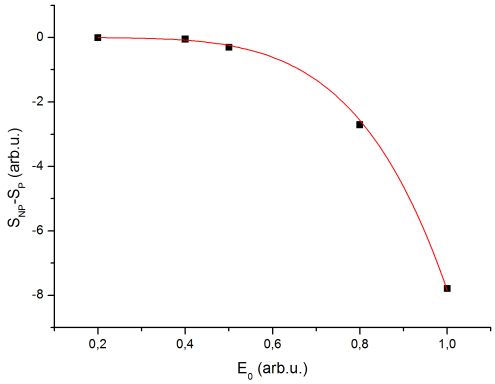

Figure 2.6: The dependence of the difference of the two-level system spectra amplitude on the electrical field amplitude. Black squares are calculated values, red line is a $\sim E_0^5$ function fit according to (2.26).

The amplitude of the difference of the spectra was evaluated for different electrical field amplitudes, see Fig. 2.6. It is clear from the figure that the difference really follows E_0^5 dependence. Notice the dependence is decreasing meaning the fifth order response has a negative value at evaluated point (center of the real part peak), see Fig. 2.3.

It was possible to directly calculated the difference of the spectra because the two calculating methods give the same resulting signal for third order response even concerning the absolute magnitude. This was verified by decreasing the electrical field amplitude E_0 and checking the fraction $\frac{P_{NP}(t)}{P_P(t)} \xrightarrow{E_0 \to 0} 1$.

If, for some reason, the absolute magnitude of the calculated spectra differed for the methods used, the spectra cannot be subtracted directly. They can be, however, divided, getting

$$\frac{S_{NP}}{S_P} = cE_0^2 + d + o(E_0^4). \tag{2.27}$$

The quadratic dependence of the fraction can then be tested. For our case, this, of course, works as well, see Fig. 2.7.

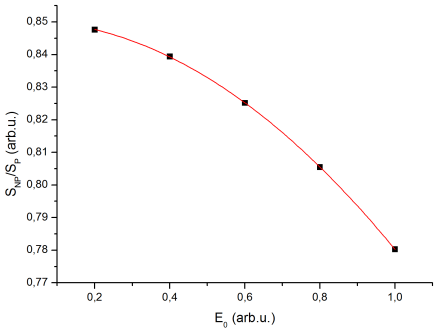

Figure 2.7: The dependence of the fraction of non-perturbatively and perturbatively calculated spectra amplitude on field amplitude. Black squares are calculated values, red line is a quadratic function fit according to (2.27).

2.2 Coupled dimer

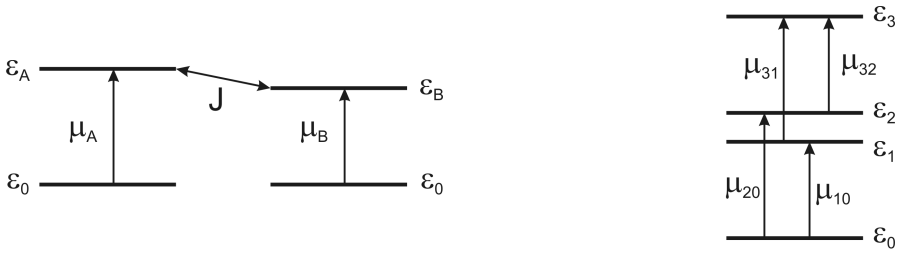

Figure 2.8: Energy levels scheme for a coupled dimer in the individual molecules basis (left) and in the excitonic basis (right)

A slightly more complicated system than two-level molecule is a coupled dimer. It consists of two two-level molecules with some coupling between their excited states, see Fig. 2.8 left. Because of this coupling, the energy levels of the dimer as a whole are shifted and, more importantly, some population transfer occurs. This gives rise to a interesting system dynamics, as described for example in [16]. A dimer can be also used as a simplest model of an antenna in a photosynthetic complex [7].

If we denote the molecules by A and B, the dimer Hamiltonian in the basis of the individual molecules ($|0\rangle$,$|A\rangle$,$|B\rangle$,$|AB\rangle$ are common ground state, molecule A, molecule B and both molecules excited state, respectively) reads

$$\begin{aligned} H_{dim} = &|0\rangle\,\varepsilon_0\,\langle 0| + |A\rangle\,\varepsilon_A\,\langle A| + |B\rangle\,\varepsilon_B\,\langle B| \\ &+ |A\rangle\,J\,\langle B| + |B\rangle\,J\,\langle A| + |AB\rangle\,(\varepsilon_A+\varepsilon_B)\,\langle AB|\,. \end{aligned} \tag{2.28}$$

Here, we excluded the kinetic energies of the nuclei and potential energy surfaces. These play important role in the interaction with the bath and will be treated phenomenologically within the Redfield theory. The dipole moment operator is

$$\mu = |A\rangle \mu_A \langle 0| + |B\rangle \mu_B \langle 0| + |AB\rangle \mu_A \langle B| + |AB\rangle \mu_B \langle A| + h.c. \tag{2.29}$$

Diagonalizing the dimer Hamiltonian with respect to energies, we obtain a so called exciton basis, which consists of a ground state $|0\rangle$, two one-exciton states $|1\rangle$ and $|2\rangle$ and one two-exciton state $|3\rangle$, see Fig. 2.8 right and Appendix B. As a result of this transformation, the energies of the one-exciton states are more distant than $\varepsilon_A - \varepsilon_B$ and the transition dipole moment operator is also transformed. Moreover, the Redfield tensor now contains some elements leading to population transfer from state $|2\rangle$ to $|1\rangle$ [16]. In principle, there would be transfer in the opposite direction as well, but assuming state $|2\rangle$ has larger energy than $|1\rangle$ it is suppressed because of detailed balance condition for transfer rates [1, 13].

2.2.1 Calculation of 2D spectrum

From this point on, we can proceed in the same way as for a two-level system. In the non-perturbative calculation, we write the equations for the density matrix (1.6) and solve them numerically, see Appendix B.1. In the perturbative approach, we have to include all relevant Liouville space pathways and integrate their response functions (1.19), see Appendix B.2. As for the two-level system, the integration step used was 1.5 fs, the RK step was 0.5 fs, the solving range was $t, \tau \in [0, 1200]$ fs and the polarization was outputted every 2 fs for both variables. The values of dimer parameters used for calculation are in Table 2.2.

Parameter	Value
$\mu_{10} = \mu_{01}$	-0.56
$\mu_{20} = \mu_{02}$	0.84
$\mu_{31} = \mu_{13}$	1.01
$\mu_{32} = \mu_{23}$	0.17
one-exciton coherence dephasing $\Gamma_{10} = \Gamma_{32}$	140 fs^{-1}
one-exciton coherence dephasing $\Gamma_{20} = \Gamma_{31}$	110 fs^{-1}
two-exciton coherence dephasing Γ_{30}	65 fs^{-1}
intraband coherence dephasing Γ_{21}	500 fs^{-1}
population relaxation $\Gamma_{11} = \Gamma_{22}$	2 ps^{-1}
population transfer rate γ_{12}	250 fs^{-1}
ω	25 000 cm^{-1}, eq. to $\lambda = 400$ nm
$\omega_{10} = \omega_{32}$	22 643 cm^{-1}
$\omega_{20} = \omega_{31}$	27 357 cm^{-1}
ω_{12}	4 714 cm^{-1}
waiting time T	700 fs
pulse width d	7 fs

Table 2.2: Parameters for coupled dimer

As in the case of the two-level system, the parameters were set to resemble a real molecular dimer.

As mentioned before, the system evolution during the waiting time T is quite complicated. Because we are interested in the calculating method, we consider an asymptotic case of large T where the coherent beating which occurs in the beginning [16] vanishes because of dephasing. Moreover, all the population of state $|2\rangle$ is transferred to state $|1\rangle$. This means only emission on lower frequency $\omega_{10} = {}^{\varepsilon_1-\varepsilon_0}/_{\hbar}$ is possible, giving rise to two positive peaks: diagonal peak 11 and a cross peak 21 (the first number denotes the excitation frequency and the second emission frequency). Applying FFT on the calculated signal, we get the desired 2D spectrum. Again, the FFT zero padding was 1200 fs. The calculated spectra are in the Fig. 2.9.

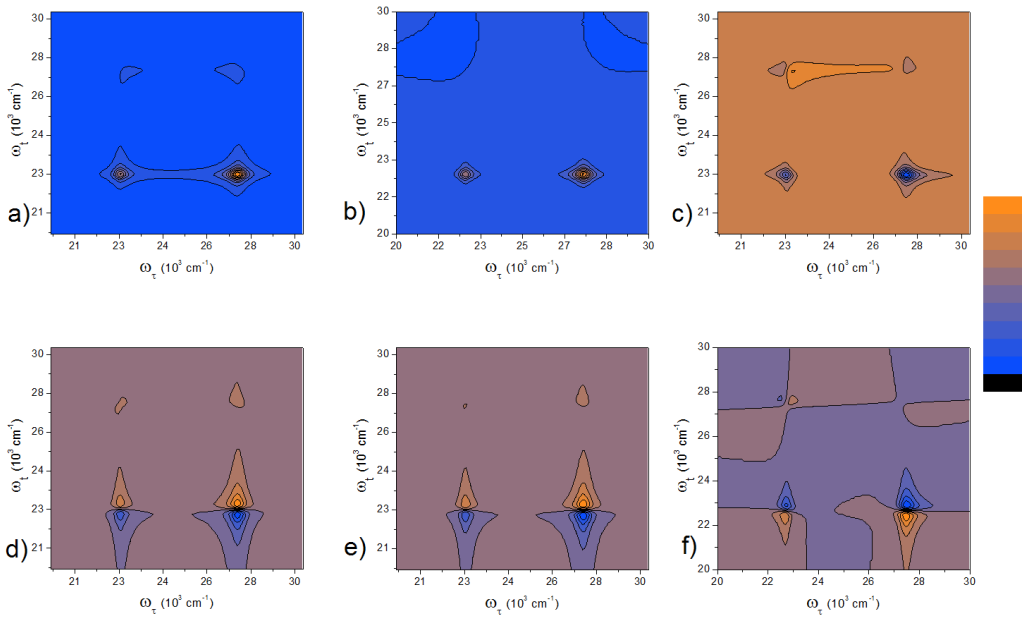

Figure 2.9: The 2D spectrum of a coupled dimer with long waiting time T calculated non-perturbatively (first column a),d)) and perturbatively (second column b),e)). In the third column there are the previous two spectra subtracted (c), f)). The first row (a),b),c)) includes the real (absorptive) part of the spectrum and the second row (d),e),f)) includes the imaginary part of the spectrum.
The contours are plotted in 10% of the overall range (from min. to max. value) intervals, blue means negative and orange positive values. The spectra were not rescaled.

As can be seen from Fig. 2.9, the perturbatively and non-perturbatively calculated spectra look much alike. Taking their difference, we note that the rule that the fifth order response has the same spectral dependence but opposite sign derived from a simple model in Section 2.1.3.1 seems to hold for the dimer as well, at least in the T large asymptotic case.

2.2.2 Order of the spectrum

To get more qualitative results, we can again test the dependence of the magnitude of the spectrum on the amplitude of the electric field as in Section 2.1.3.2. The perturbatively calculated spectrum inherently depends on E_0^3, while the non-perturbatively calculated one behaves not necessarily exactly as E_0^3. The dependence of non-perturbatively calculated spectrum magnitude $S_{NP}(E_0)$ is in Fig. 2.10

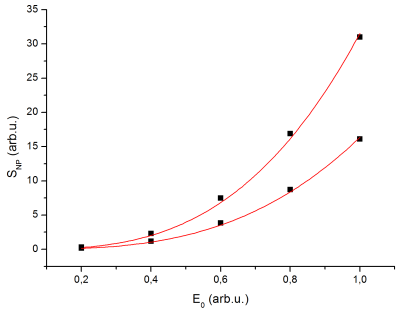

Figure 2.10: The dependence of non-perturbatively calculated signal amplitude on field amplitude. Black squares are calculated values, red lines are cubic functions fits according to (2.24). The two curves correspond to two different chosen points (maximum of 21 peak in real part of the spectrum and maximum of positive part of 21 peak in imaginary part of the spectrum).

As can be seen from Fig. 2.10, the dependence is mainly E_0^3, but with slight deviation. In the same way as for the two-level system, this deviation can be explained by means of the presence of higher order polarization contributions in the non-perturbatively calculated spectrum. The amplitude of the difference of the spectra was evaluated for different electric field amplitudes, see Fig. 2.11.

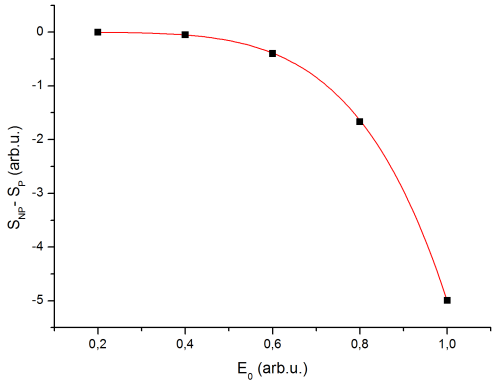

Figure 2.11: The dependence of the difference of the dimer spectra amplitude on the electrical field amplitude. Black squares are calculated values, red line is a $\sim E_0^5$ function fit according to (2.26).

As can be seen from the figure, the dependence indeed is $\sim E_0^5$. Notice the dependence is decreasing meaning the fifth order response has a negative value at evaluated point (center of the 21 real peak), see Fig. 2.9. Another option to prove the presence of the fifth order is, again, to divide the spectra, exploiting the (2.27) quadratic dependence. The result is in Fig. 2.12.

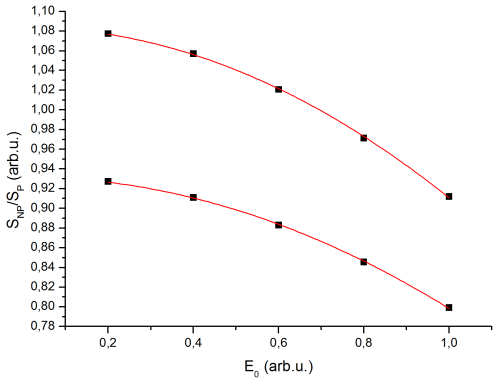

Figure 2.12: The dependence of the fraction of non-perturbatively and perturbatively calculated spectra amplitude on field amplitude. Black squares are calculated values, red line is a quadratic function fit according to (2.27).The two curves correspond to the two points described in Fig. 2.10.

Conclusion

In this thesis the perturbative and non-perturbative approaches to the calculation of a 2D spectrum were described. The main advantage of the perturbative approach is its intuitive description, while for even a little more complicated systems such as a coupled dimer, the number of Liouville pathways necessary to include becomes exhausting. The computational effort is significantly increased as well. Here, the non-perturbative calculation proves to be more straightforward. However, one obtains the spectrum as a whole with only a limited possibility to probe individual features. We find it therefore more useful to calculate the whole spectrum non-perturbatively, and to attempt the interpretation in a perturbative language, optionally calculating a contribution of some individual Liouville space pathways of interest.

The perturbative and non-perturbative calculations were carried out for two model systems: a two-level molecule and a coupled dimer. The resulting spectra were compared. It was found that the non-perturbatively calculated spectrum contains also contributions from higher order of polarization. When calculating a 2D spectrum, it it thus important to ensure the external electric field is sufficiently weak in order to make sure the higher order nonlinearities remain negligible. For the Markovian bath, this was the only difference found. However, when including a memory of the bath, additional differences should arise because of different treatment of the bath in perturbative and non-perturbative approach. This is therefore one possible direction in which to look for further comparison of the two approaches considered.

Bibliography

[1] Butkus, V., Abramavicius, D., Gelzinis, A., and Valkunas, L., Two-dimensional optical spectroscopy of molecular aggregates. *Lith. J. Phys.* 2010, *50*(3), 267.

[2] Collini, E. and Scholes, G. D., Coherent intrachain energy migration in a conjugated polymer at room temperature. *Science* 2009, *323*, 369.

[3] Engel, G. S., Calhoun, T. R., Read, E. L., Ahn, T.-K., Mančal, T., Cheng, Y.-C., Blankenship, R. E., and Fleming, G. R., Evidence for wavelike energy transfer through quantum coherence in photosynthetic systems. *Nature* 2007, *446*, 782.

[4] Frigo, M. and Johnson, S. G., FFTW Fast Fourier Transform subroutine library. `http://www.fftw.org`.

[5] Gelin, M. F., Egorova, D., and Domcke, W., Efficient method for the calculation of time- and frequency-resolved four-wave mixing signals and its application to photon-echo spectroscopy. *J. Chem. Phys.* 2005, *123*, 164112.

[6] Hamm, P. and Zanni, M., *Concepts and methods of 2d infrared spectroscopy*. Cambridge: Cambridge University Press 2011.

[7] Mančal, T., Primární procesy ve fotosyntéze Od buňky ke kvantové superpozici a zpět . *Čs.čas.fyz.* 2011, *61*(3), 151.

[8] Mančal, T., Pisliakov, A. V., and Fleming, G. R., Two-dimensional optical three-pulse photon echo spectroscopy. I. Nonperturbative approach to the calculation of spectra. *J. Chem. Phys.* 2006, *124*(23), 234504.

[9] Mančal, T., Bixner, O., Christensson, N., Haurer, J., Milota, F., Nemeth, A., Sperling, J., and Kauffmann, H., Dynamics of quantum wave packets in complex molecules traced by 2D coherent electronic correlation spectroscopy . *Procedia Chemistry* 2011, *3*, 105.

[10] Mančal, T. and Šanda, F., Quantum master equations for non-linear optical response of molecular systems. *Chem. Phys. Lett.* 2012, *530*, 140.

[11] May, V. and Kühn, O., *Charge and energy transfer dynamics in molecular systems*. Berlin: Wiley-VCH 2001.

[12] Milota, F., Sperling, J., Nemeth, A., Mančal, T., and Kauffmann, H. F., Two-dimensional electronic spectroscopy of molecular excitons. *Acc. Chem. Res.* 2009, *42*(9), 1364.

[13] Mukamel, S., *Principles of nonlinear spectroscopy*. Oxford: Oxford University Press 1995.

[14] Olšina, J. and Mančal, T., Parametric projection operator technique for second order non-linear response. *J. Chem. Phys.* 2012, *accepted*.

[15] Panitchayangkoona, G., Hayesa, D., Fransteda, K. A., Carama, J. R., Harela, E., Wenb, J., Blankenship, R. E., and Engel, G. S., Long-lived quantum coherence in photosynthetic complexes at physiological temperature. *Proc. Natl. Acad. Sci. U. S. A.* 2010, *107*(29), 12766.

[16] Pisliakov, A. V., Mančal, T., and Fleming, G. R., Two-dimensional optical three-pulse photon echo spectroscopy. II. Signatures of coherent electronic motion and exciton population transfer in dimer two-dimensional spectra. *J. Chem. Phys.* 2006, *124*(23), 234505.

[17] Stone, K. W., Gundogdu, K., Turner, D. B., Li, X., Cundiff, S. T., and Nelson, K. A., Two-Quantum 2D FT Electronic Spectroscopy of Biexcitons in GaAs Quantum Wells . *Science* 2009, *324*, 1169.

[18] Zigmantas, D., Read, E. L., Mančal, T., Brixner, T., Gardiner, A. T., Cogdell, R. J., and Fleming, G. R., Two-dimensional electronic spectroscopy of the B800–B820 light-harvesting complex. *Proc. Natl. Acad. Sci. U. S. A.* 2006, *103*(34), 12672.

A. Two-level system

A.1 Bloch equations

Here, we present an exact solution of equations (2.12), (2.13) and (2.14) for delta-function pulses form of electrical field. During the calculation we divide the time axis into four sections according to the pulses (2.9) ($t < -T-\tau$, $-T-\tau < t < -T$, $-T < t < 0$, $0 < t$). This corresponds to time-localized interaction with the laser pulses and free propagation between the interactions. In each section we take the values from the previous section as an initial condition and the factor in front of the delta function determines the jump of the appropriate density matrix element. Because the equations are coupled, the values of ρ_{gg} and ρ_{ee} determine the jump of σ_{eg} and vice versa. We use the values of the populations ρ_{gg} and ρ_{ee} as a first initial condition, jump with the coherences σ_{eg} and then change the populations, using the σ_{eg} value as a new initial condition. Because in the equations $\hbar$ occurs only accompanied by μ, we set $\hbar = 1$ for the following calculations and in the end use $\mu \to \frac{\mu}{\hbar}$.

For the the zeroth section $t < -T - \tau$ we use ground state equilibrium initial conditions: $\rho^0_{gg} = 1,\ \rho^0_{ee} = \sigma^0_{eg} = 0$.

Plugging the zeroth section into Eqs. (2.12), (2.13) and (2.14) we get for the first section $-T - \tau < t < -T$

$$\sigma^1_{eg} = i\mu_{eg} e^{i\Phi_1 - i\omega(T+\tau)} \theta(t+T+\tau) e^{-i(\omega_{eg}-\omega)(T+\tau)-\Gamma(T+\tau)} e^{-i(\omega_{eg}-\omega)t-\Gamma t}, \tag{A.1}$$

$$\rho^1_{gg} = 1 - |\mu_{eg}|^2 \theta(t+T+\tau), \tag{A.2}$$

$$\rho^1_{ee} = |\mu_{eg}|^2 \theta(t+T+\tau). \tag{A.3}$$

Here, we used only a half of the right limit of σ_{eg} because of the theta function accompanying it, saying basically that "$\theta\delta = \frac{1}{2}\delta$" under the integration sign.

Now, using the first section results we solve in the second section $-T < t < 0$

$$\begin{aligned} \sigma^2_{eg} \quad = \tfrac{i}{\hbar}\mu_{eg}[e^{i\Phi_1 - i\omega(T+\tau)} e^{-i(\omega_{eg}-\omega)\tau-\Gamma\tau} + e^{i\Phi_2 - i\omega T}(1 - 2|\mu_{eg}|^2)\theta(t+T)] \\ e^{-i(\omega_{eg}-\omega)T-\Gamma T} e^{-i(\omega_{eg}-\omega)t-\Gamma t}, \end{aligned} \tag{A.4}$$

$$\begin{aligned} \rho^2_{gg} = \quad (1 - |\mu_{eg}|^2) - |\mu_{eg}|^2[e^{-i\Phi_1 + i\omega(T+\tau) + i\Phi_2 - i\omega T + i(\omega_{eg}-\omega)\tau - \Gamma\tau} + \\ +2(1 - 2|\mu_{eg}|^2) + e^{i\Phi_1 - i\omega(T+\tau) - i\Phi_2 + i\omega T - i(\omega_{eg}-\omega)\tau - \Gamma\tau}]\theta(t+T), \end{aligned} \tag{A.5}$$

$$\rho^2_{ee} = \{|\mu_{eg}|^2 + |\mu_{eg}|^2[e^{-i\Phi_1+i\omega(T+\tau)+i\Phi_2-i\omega T+i(\omega_{eg}-\omega)\tau-\Gamma\tau} +2(1-|\mu_{eg}|^2) + e^{i\Phi_1-i\omega(T+\tau)-i\Phi_2+i\omega T-i(\omega_{eg}-\omega)\tau-\Gamma\tau}]\theta(t+T)\}. \tag{A.6}$$

Finally, in the last section for $t > 0$ we are interested only in the off-diagonal element

$$\sigma^3_{eg} = i\mu_{eg}\{e^{i\Phi_1-i\omega(T+\tau)}e^{-i(\omega_{eg}-\omega)(T+\tau)-\Gamma(T+\tau)} + +e^{i\Phi_2-i\omega T-i(\omega_{eg}-\omega)T-\Gamma T}(1-2|\mu_{eg}|^2) + [1-2|\mu_{eg}|^2 -|\mu_{eg}|^2(e^{-i\Phi_1+i\Phi_2+i\Phi_3+i\omega\tau+i(\omega_{eg}-\omega)\tau-\Gamma\tau} + 2(1-|\mu_{eg}|^2) + c.c.)]2\theta(t)\} \times e^{-i(\omega_{eg}-\omega)t-\Gamma t}. \tag{A.7}$$

Extracting the term with the required phase $\Phi = -\Phi_1 + \Phi_2 + \Phi_3$ and returning to $\hbar$, we get

$$\sigma^{\Phi}_{eg}(t) = \theta(t)\theta(T)\theta(\tau)\frac{-i\mu_{eg}|\mu_{eg}|^2}{\hbar^3}2e^{-i\omega_{eg}(t-\tau)-\Gamma(t+\tau)}e^{i\omega t}, \tag{A.8}$$

which is (2.17). Here, we added the theta functions, for the calculation is valid only for the ordering of the interactions where $t > 0$, $T > 0$, $\tau > 0$. For $\tau < 0$ the process is practically the same with the first and second sections switched. The result is a non-rephasing response.

B. Coupled dimer

Here, the transformation of the dimer Hamiltonian and dipole moment operator from local excited state basis to excitonic basis is presented. Only the energies are included in the Hamiltonian, nuclear potential energy surfaces transformation leading to dephasing and population transfer are treated within the Redfield theory [11, 16]. The individual molecules basis reads $\{|0\rangle, |A\rangle, |B\rangle, |AB\rangle\}$ denoting which molecule is excited. The Hamiltonian in this basis has a matrix form

$$H_{mol} = \begin{pmatrix} \varepsilon_0 & 0 & 0 & 0 \\ 0 & \varepsilon_A & J & 0 \\ 0 & J & \varepsilon_B & 0 \\ 0 & 0 & 0 & \varepsilon_A + \varepsilon_B \end{pmatrix} \tag{B.1}$$

and the dipole moment operator reads

$$\begin{pmatrix} 0 & \mu_A & \mu_B & 0 \\ \mu_A & 0 & 0 & \mu_B \\ \mu_B & 0 & 0 & \mu_A \\ 0 & \mu_B & \mu_A & 0 \end{pmatrix}. \tag{B.2}$$

The excitonic basis reads $\{|0\rangle, |1\rangle, |2\rangle, |3\rangle\}$. The Hamiltonian in this basis is diagonal in energies and is obtained by appropriate transformation of (B.1)

$$H_{exc} = \mathcal{Q} H_{mol} \mathcal{Q}^{\dagger}, \tag{B.3}$$

$$H_{exc} = \begin{pmatrix} \varepsilon_0 & 0 & 0 & 0 \\ 0 & \varepsilon_1 & 0 & 0 \\ 0 & 0 & \varepsilon_2 & 0 \\ 0 & 0 & 0 & \varepsilon_A + \varepsilon_B \end{pmatrix}, \tag{B.4}$$

$$\mathcal{Q} = \begin{pmatrix} 1 & 0 & 0 & 0 \\ 0 & -sin\vartheta & cos\vartheta & 0 \\ 0 & cos\vartheta & sin\vartheta & 0 \\ 0 & 0 & 0 & 1 \end{pmatrix}, \tag{B.5}$$

where

$$tan(\vartheta) = \frac{2J}{\varepsilon_A - \varepsilon_B}. \tag{B.6}$$

The dipole moment operator transforms in a similar fashion, yielding ($c\vartheta = cos\vartheta$, $s\vartheta = sin\vartheta$

$$\begin{pmatrix} 0 & -\mu_A s\vartheta + \mu_B c\vartheta & \mu_A c\vartheta + \mu_B s\vartheta & 0 \\ -\mu_A s\vartheta + \mu_B c\vartheta & 0 & 0 & \mu_A c\vartheta - \mu_B s\vartheta \\ \mu_A c\vartheta + \mu_B s\vartheta & 0 & 0 & \mu_A s\vartheta + \mu_B c\vartheta \\ 0 & \mu_A c\vartheta - \mu_B s\vartheta & \mu_A s\vartheta + \mu_B c\vartheta & 0 \end{pmatrix}. \quad \text{(B.7)}$$

By transforming the nuclear potentials and taking into account the Redfield theory with some model of a bath [16], the population relaxation, coherence dephasing and population transfer rates can be obtained. As the system-bath interaction is not of main interest in this thesis, we introduced these rates phenomenologically.

B.1 Non-perturbative approach

In the excitonic basis, we can write the equations of motion for the density matrix (1.6). According to the RWA we use an ansatz $\rho_{10} = \sigma_{10}e^{-i\omega t}$, $\rho_{31} = \sigma_{31}e^{-i\omega t}$, $\rho_{30} = \sigma_{30}e^{-i2\omega t}$ and the same for $1 \leftrightarrow 2$. The electrical field is in the form (1.9). Then, we neglect terms oscillating as rapidly as $\sim e^{\pm i\omega t}$. The transition frequencies are defined as $\omega_{ij} = {}^{\varepsilon_i - \varepsilon_j}/_{\hbar}$. As in the case of the two-level system, we set $\hbar = 1$. The equations of motion for the elements of RDM read

$$\frac{\partial \sigma_{10}}{\partial t} = -i(\omega_{10} - \omega)\sigma_{10} - \Gamma_{10}\sigma_{10} + iE(t)(\mu_{10}(\rho_{00} - \rho_{11}) - \mu_{20}\rho_{12}) + iE^*(t)\mu_{31}\sigma_{30}, \quad \text{(B.8)}$$

$$\frac{\partial \sigma_{31}}{\partial t} = -i(\omega_{31} - \omega)\sigma_{31} - \Gamma_{31}\sigma_{31} + iE(t)(\mu_{31}\rho_{11} + \mu_{32}\rho_{21} - \mu_{31}\rho_{33}) - iE^*(t)\mu_{10}\sigma_{30}, \quad \text{(B.9)}$$

$$\frac{\partial \sigma_{30}}{\partial t} = -i(\omega_{30} - 2\omega)\sigma_{30} - \Gamma_{30}\sigma_{30} + iE(t)(\mu_{31}\sigma_{10} + \mu_{32}\sigma_{20} - \mu_{10}\sigma_{31} - \mu_{20}\sigma_{32}), \quad \text{(B.10)}$$

$$\frac{\partial \rho_{21}}{\partial t} = -i\omega_{21}\rho_{21} - \Gamma_{21}\rho_{21} + iE(t)(\mu_{20}\sigma_{01} - \mu_{31}\rho_{23}) + iE^*(t)(\mu_{23}\sigma_{31} - \mu_{01}\sigma_{20}), \quad \text{(B.11)}$$

$$\frac{\partial \rho_{11}}{\partial t} = -\Gamma_{11}\rho_{11} + \gamma_{12}\rho_{22} + iE(t)(\mu_{10}\sigma_{01} - \mu_{31}\rho_{13}) + iE^*(t)(\mu_{31}\sigma_{31} - \mu_{10}\sigma_{10}), \quad \text{(B.12)}$$

$$\frac{\partial \rho_{00}}{\partial t} = -iE(t)(\mu_{10}\sigma_{01} + \mu_{20}\rho_{02}) + iE^*(t)(\mu_{10}\sigma_{10} + \mu_{20}\sigma_{20}), \quad \text{(B.13)}$$

$$\frac{\partial \rho_{33}}{\partial t} = -\Gamma_{33}\rho_{33} + iE(t)(\mu_{31}\sigma_{13} + \mu_{32}\sigma_{23}) - iE^*(t)(\mu_{13}\sigma_{31} + \mu_{23}\sigma_{32}). \quad \text{(B.14)}$$

The remaining equations for σ_{20}, σ_{32} and ρ_{22} are obtained by replacing $1 \leftrightarrow 2$. The Γ_{ij} are population relaxation ($i = j$) and coherence dephasing ($i \neq j$) rates, γ_{12} is a population transfer rate from state $|2\rangle$ to state $|1\rangle$.

The equations (B.8) to (B.14) are the same as in [16], only the presence of element ρ_{33} makes a difference. We can, however, show that for the third order response, the ρ_{33} state is never populated. For this, we need the perturbative language. This is therefore a typical situation where the intuitive perturbative approach is used to impose an additional knowledge on the computationally more effective non-perturbative approach making it even more efficient.

B.2 Perturbative approach

In the perturbative approach, all the possible Liouville space pathways must be included and integrated (1.19). As can be seen from the double sided Feynman diagrams, the double coherence response $S^{(3)}_{DC}$ are present only when the pulse with wave vector $\mathbf{k}_1$ arrives last. Keeping the order of the pulses with the $\mathbf{k}_3$ pulse last thus eliminates some of the possible pathways simplifying the problem a little. Still, there remain several possible pathways, as listed in Fig. B.1.

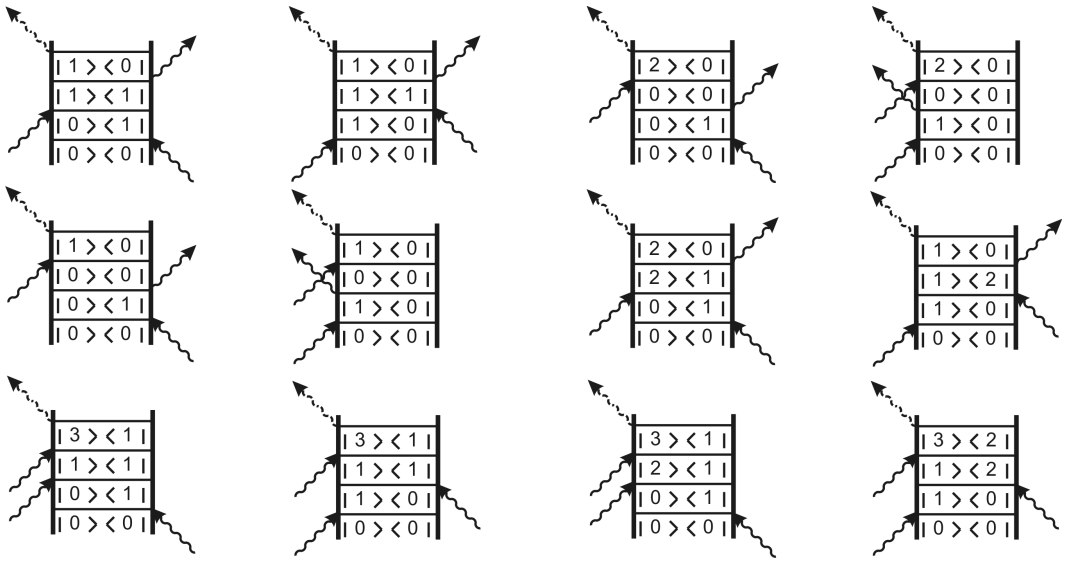

Figure B.1: Possible Liouville space pathways for coupled dimer, without population transfer. For every diagram there exists one more diagram with substitution $1 \leftrightarrow 2$

When including population transfer between population of $|2\rangle\langle 2|$ and $|1\rangle\langle 1|$, more Liouville space pathways are possible, see Fig. B.2.

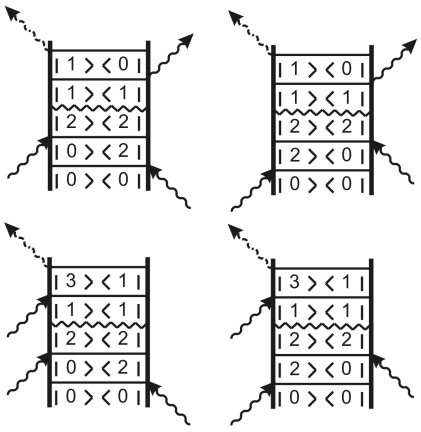

Figure B.2: Possible Liouville space pathways four coupled dimer with downward population transfer $2 \rightarrow 1$ indicated by zig-zag line. The transfer upward is negligible because of detailed balance.